Submitted for publication in ApJ
Preprint typeset using LaTeX style emulateapj v. 12/16/11

THE CONNECTION BETWEEN STAR FORMATION RATE AND DARK MATTER HALO MASS IN THE EPOCH OF REIONIZATION

Felipe L. Gomez-Cortes, Jaime E. Forero-Romero
Departamento de Física, Universidad de los Andes, Cra. 1 No. 18A-10, Edificio Ip, Bogotá, Colombia
Submitted for publication in ApJ

ABSTRACT

We present updated constraints on the relationship between the star formation rate and dark matter halo mass at redshift $z \sim 6$. The observational basis for our work is the restframe UV luminosity function data obtained with CFHTLS, HST Legacy Survey and UKIDSS. The constraints are based on an abundance matching methodology to the observational data using cosmological N-body simulations. We also take into account the influence on the results of the dust extinction scaling derived from observations by Bouwens. We show dependence of our parameter uncertainties related to the comoving volume and magnitude range in observed surveys, taking advantage of the wide mass resolution range of latest available dark matter halo catalogs. We compare our results against the results of abundance matching methods (to the stellar mass), a semi-analytic model of galaxy formation (GALFORM) and a hydrodynamical simulation (Illustris).

Subject headings: galaxies: high-redshift — methods: numerical

1. INTRODUCTION

All magnitudes are in AB system.

2. OBSERVATIONAL DATASETS

We use information from seven observational data sets. Four obtained with the Hubble Space Telescope (HST) and three from ground-based telescopes. All of them select galaxy candidates at $z \sim 6$ using the drop-out technique (Steidel et al. 1996).

The data from the Hubble Space Telescope Legacy (HSTL) (Bouwens et al. 2015) is a compilation of observations since the installation of the Advanced Camera for Surveys (ACS) in 2002, through the near-infrared Wide Field Camera 3 (WFC3/IR) installed in 2009, up to 2012.

The HST fields of view are: XDF, HUDF09-1, HUDF09-2, CANDELS-S/Deep, CANDELS-S/Wide, ERS, CANDELS-N/Deep, CANDELS-N/Wide, CANDELS-UDS, CANDELS-COSMOS and CANDELS-EGS, with areas of 4.7, 4.7, 4.7, 64.5, 34.2, 40.5, 62.9, 60.9, 151.2, 151.9 and 150.7 arcmin^2 respectively. The total area at redshift 6 corresponds to 740.8 arcmin^2 over five different lines of sight, wit a total volume of 1.8×10^6Mpc^3. Two cameras performed the observations: ACS and WFC3/IR, using B_{435}, V_{606}, i_{814}, z_{850}, I_{814}, Y_{098}, Y_{105}, $J125$, JH_{140} and H_{160} filters. The limit magnitude is between $\sim$ 27.5mag in CANDELS-EGS and$\sim$ 30mag in the deepest field (XDF). Total number of z=6 LBG candidates is 940, most of them in the faint end of the LF, magnitudes in the rest frame are in the range $-22.52 \leq M_{1600} \leq -16.77$ Bouwens et al. (2015) calculated LF using a stepwise maximum-likelihood (SWML) based on Efstathiou et al. (1988). The Schechter parameters derived are: $\phi^* = (0.33^{+0.15}_{-0.10}) \times 10^{-3}$Mpc^{-3}, $M^*_{1600} = -21.16 \pm 0.20$ and $\alpha = -1.91 \pm 0.09$. Bouwens et al. (2015) reported that using just few fields of view, UVLF has a slightly non-Schechter-like form.

Finkelstein et al. (2014) worked also with HST, using the HUDF, CANDELS and GOODS fields, along with two of the Hubble Frontier Fields (HFF): deep parallel observations (unlensed fields) near the Abell 2744 and MACS J0416.1-2403 clusters. The HFF uses the ACS and the WFC3/IR with the same filters aforementioned but z_{850}. Total survey area is around $\sim$ 300arcmin^2, with 706 photometric candidates at redshift 6 defined as the interval $5.5 < z < 6.5$. Total volume of this study is around 8×10^5Mpc^3. The Schechter function parameters they found are $\phi^* = (1.86^{+0.94}_{-0.80}) \times 10^{-4}$Mpc^{-3}, $M^*_{1600} = -21.1^{+0.25}_{-0.31}$ and $\alpha = -2.02^{+0.10}_{-0.10}$.

Willott et al. (2013) presented the sixth release of the Canada-France-Hawaii Telescope Legacy Survey CFHTLS. The observations where performed over four separated fields covering a total area $\sim 4\,\mathrm{deg}^2$ (a large area), it gives this survey great robustness. Optical observations used MegaCam with $u^*g'r'i'z'$ filters. The main selection criteria: all the objects must be brighter than magnitude $z' = 25.3$. The final number of LBGs founded was 40. Moreover, they get spectroscopic confirmation for 7 candidates using GMOS spectrograph on the Gemini Telescopes, which has a $\ll$ 5.5-square arcmin field of view, giving a volume $\sim 1.09 \times 10^7$Mpc^3. They show incompleteness in the sample due to foreground contamination and the detection algorithm; there is no warranty to have every object brighter than the limit magnitude on the faint limit. The full galaxy LF at $z = 6$ cannot be obtained as in other studies. Nevertheless, this survey was focussed on the highly luminous LBGs. LF is calculated using the stepwise maximum likelihood method of Efstathiou et al. (1988), within magnitudes from $M_{1350} = -22.5$ up to -20.5. The luminosity function of $z = 5.9$ shows an exponential decline at the bright end, where feedback processes and inefficient last cooling limites star forming in bright galaxies hosted in the most massive halos.

fl.gomez10@uniandes.edu.co
je.forero@uniandes.edu.co

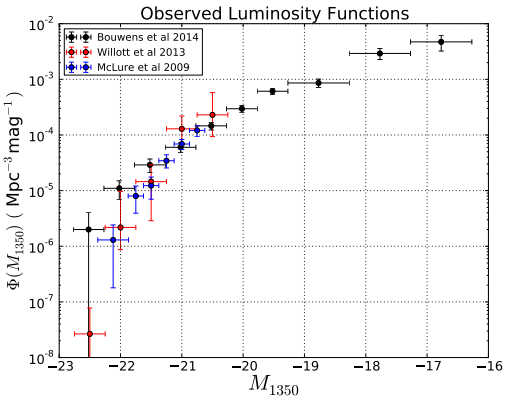

FIG. 1.— Observational data from Bouwens et al. (2015); McLure et al. (2009)and Willott et al. (2013).

McLure et al. (2009) build the luminosity function for $z = 5$ and $z = 6$ using data from two ground-based telescopes: the United Kingdom Infrared Telescope in the near-IR imaging and Subaru Telescope for the optical imaging. They use the first data release of the UKIRT Infrared DeepSky Survey Ultra Deep Survey (UDS), together with the Subaru XMM-Newton Survey (SXDS). Total observed area is $0.63\,\mathrm{deg}^2$ uniformly covered by booth catalogues. The volume in this survey is $\sim 3 \times 10^6 \mathrm{Mpc}^3$. The UKIRT was equipped with the WFCAM using JK filters. The Subaru was equipped with the Suprime-Cam with the $BVRi'z'$ filters. All candidates where brighter than $z' = 26$. The UV rest frame magnitude range is $-22.4 \leq M_{1500} \leq -20.6$. The LF was calculated using the maximum likelihood estimator of Schmidt (1968). Their analysis gave a total number of 104 LBG candidates in the redshift range $5.7 \leq z \leq 6.3$. LF was parameterized according to the Schechter function with $\phi^* = (1.8 \pm 0.5) \times 10^{-3}\mathrm{Mpc}^{-3}$, $M^*_{1500} = -20.04 \pm 0.12$ and $\alpha = -1.71 \pm 0.11$.

The dataset was retrieved from McLure et al. (2009) graph using GAVO-DEXTER[1].

3. ABUNDANCE MATCHING METHODOLOGY

The relation between UV luminosity and Star Formation Rate (Madau et al. 1998; Kennicutt 1998) is given by:

$$\mathrm{SFR}\left(M_\odot \mathrm{yr}^{-1}\right) = 1.4 \times 10^{-28} L_\nu \left(\mathrm{erg\ s^{-1} Hz^{-1}}\right) \quad (1)$$

With Initial Mass Function (IMF) between $0.1M_\odot$ and $100M_\odot$, in the range of $1250 - 2500$Å

The star forming rate will be:

$$SFR = k \times L_0 M \left[\left(\frac{M}{M_0}\right)^{-\beta} + \left(\frac{M}{M_0}\right)^{\gamma} \right]^{-1} \quad (2)$$

The key element to connect SFR with halo mass from simulations is the observed UVLF. If there exist a function whom gives to each halo a UV luminosity then is posible to reproduce UVLF from DMH catalogs. The fitting parameters can be explored using a Markov Chain Monte-Carlo (MCMC) implementation. Once the parameters are found, the SFR-Halo Mass relation have been found.

We use the dark matter halo catalog from the Big MultiDark Plank 1 (MDPL) Simulation (Klypin et al. 2014) with 2013 Planck cosmology (Planck Collaboration et al. 2014). MDPL is quite similar to the Big Bolshoi ($1\mathrm{Gpc\ h}^{-1}$) (Prada et al. 2012) and its predecesor Bolshoi (Klypin et al. 2011) ($250\mathrm{Mpc\ h}^{-1}$), booth of them with WMAP5 cosmology, but MDPL has bigger mass resolution. Those halo catalogs are available at the MultiDark Database[2] (Riebe et al. 2013).

The MDPL run is a N-body dark matter only simulation based on the L-Gadget2 code. The simulated volume is a cubic box of $1\mathrm{Gpc\ h}^{-1}$ side length. It has 3840^3 dark matter particles of $1.51 \times 9\mathrm{M}_\odot\mathrm{h}^{-1}$ mass each one. The 2013 Planck cosmology is defined by the following parameters: $\Omega_M = 0.307$, $\Omega_B = 0.048$, $\Omega_\Lambda = 0.730$, $\sigma_8 = 0.829$, $n_s = 0.96$ and $H_0 = 67.8$. The DMH Catalog at $z = 6$ contains $\sim 10.9 \times 10^7$ halos, to avoid incompleteness in the low mass end, halos with mass below $10^{10.3}\mathrm{M}_\odot\mathrm{h}^{-1}$ are rejected. In order to study how cosmic variance can affect measurements, the original catalog is divided into 64 small cubic boxes, with a similar volume to the observations.

The following treatment is applied to every one small box.

The halo abundance matching technique has been widely used (Colín et al. 1999; Kravtsov et al. 2004) resulting in good reproduction of the observed galaxy clustering. (Conroy et al. 2006; Lee et al. 2009). Here we use the simplest case with few premises:

1. Each halo in the catalog hosts one galaxy. There are not empty halos, also none of halos has two or more galaxies.

2. The UV luminosity of each galaxy is function of one variable; the mass of the DMH in which is located. This function must be monotone, this guarantees that most massive halos will host the most luminous galaxies in the same volume.

3.1. *Fitting Model*

The observed UV Luminosity Function has two slopes. To reproduce it we decide to use the four parameter model:

$$L_{\mathrm{UV}}(M) = L_0 M \left[\left(\frac{M}{M_0}\right)^{-\beta} + \left(\frac{M}{M_0}\right)^{\gamma} \right]^{-1} \quad (3)$$

where M is the hosting DMH mass, L_0 is a normalization constant, M_0 is the critical mass where the luminosity function has a slope change, β and γ are the slopes. This equation has a similar fashion to the mass to light relation (van den Bosch et al. 2003) and the mean relation between stellar mas of a galaxy and the mass of its halo used by Moster et al. (2010).

3.2. *Dust Attenuation*

Dust in star forming galaxies absorbs part of the UV radiation and reemits on IR. The more massive is the

[1] http://dc.zah.uni-heidelberg.de/dexter/ui/ui/custom

[2] http://www.multidark.org

galaxy then more dust contains and dust attenuation will be greater. The relation between dust attenuation and magnitude have been already studied, with this relation we can infer the dust-free UV luminosity of a galaxy from observations, resulting in a more accurate inferred SFR.

The UV Spectral Slope β was introduced by Meurer et al. (1999) as a UV color to study dust attenuation in local starburst galaxies and extrapolating to high redshift galaxies. This index appears when a power law fitting is performed over the spectral flux f as function of the wavelength λ;

$$f \propto \lambda^{\beta}.$$

The relation for ultra-violet attenuation at 1600Å they found is:

$$A_{1600} = 4.43 + 1.99\beta, \tag{4}$$

with A_{1600} in magnitude units.

Due LBGs have more similar spectra properties to local starburst galaxies rather than AGNs for example, we can assume that local calibration of $\beta - A_{1600}$ can be applied also for LBGs, "The main requirement is that the data include fluxes in two broad bands or coarse spectra covering the rest-frame UV."

Bouwens et al. (2012) uses the fluxes on different bands to estimate β on each LBG candidate found with $z \sim 4-7$. After in redshift groups they found a linear relation between β and the UV magnitude:

$$\langle\beta\rangle = \frac{d\beta}{dM_{UV}}\left(M_{UV,AB} + 19.5\right) + \beta_{M_{UV}=-19.5} \tag{5}$$

with $\beta_{M_{UV}=-19.5} = -2.20$ and $d\beta/dM_{UV} = -0.21$ at $z = 5.9$.

Smit et al. (2012) used the aforementioned relations to infer the corrected luminosity functions, i.e. dust-free luminosity functions, and the corrected SFR at $z = 4$.

Here we use the inverse relation, starting from the intrinsic or dust-free galaxy magnitude, obtaining the observed magnitude:

$$M_{obs} = \begin{cases} \frac{M_{int}-4.616}{1.259}, & \text{if } A > 0 \\ M_{int}, & \text{else} \end{cases}. \tag{6}$$

3.3. *MCMC*

We used a Markov Chain Monte Carlo method to find the best parameters and its uncertainties over each one of the boxes and each observational dataset. The code was written on Python using the SciPy Library (Jones et al. 2001–) the IPython environment (Pérez & Granger 2007).

First of all, one of the four observational data sets (Bouwens, Finkelstein, Willott and McLure) is selected to be the model to fit. From the whole simulated halo catalog, a subsample with cubic box shape of 250Mpc h^{-1} length is selected.

With an initial set of parameters (α, γ, M_0, and L_0) the UV luminosity for the halo is calculated as function of his mass according to equation 3. Then Luminosity is converted to magnitude units using:

$$M_{UV} = 51.82 - 2.5\log_{10}(L_{UV}).$$

If we consider the dust attenuation im the equation 6 we have a dust-corrected UV Luminosity Function.

The luminosity function is constructed as an histogram of the magnitudes normalized by the volume of the catalog. Each observed luminosity function has a different bin range.

Once having the LF, we compare our LF against observed LF. The error function we consider is the sum of the square difference over each bin, divided by the observational data uncertain.

$$\chi^2 = \sum_{i=o}^{n} \frac{\left(x_{i,obs} - x_{i,fit}\right)^2}{2\sigma_i^2}$$

We worked on the logarithmic space of luminosities to have a good fitting on six decades.

The likelihood will have this property:

$$\mathcal{L} \propto \exp\left(-\frac{\chi^2}{n}\right)$$

, where n is the number of degrees of freedom. We have the maximum likelihood when the error is the minimum.

Each MCMC step will have have a small variation of the parameters, the UV luminosity and magnitude are calculated again for each halo, we have a new error χ^2_{new} and a new likelihood $\mathcal{L}_{new}$.

Following the Metropolis method, we compare the new and the old likelihood:

$$R = \frac{\mathcal{L}_{new}}{\mathcal{L}_{old}} = exp(\chi^2_{new} - \chi^2_{old})$$

If $R \geq 1$, then we immediate accept the new set of parameters and start the next MCMC step.

Else, we have a chance to keep the new set. When $R < 1$, we compare with a uniformly random number p in the range $[0, 1]$. if $R > p$ we accept the new set of parameters and start the next MCMC step. Else we reject the new set and start again with the old set.

We performed 100.000 effective MCMC steps, plus 10.000 thermalization steps over each box. We repeated for the same box without consider dust attenuation.

Then we perform the same method over the 64 boxes and the resting three data sets.

The restrictions imposed over the parameters where $0 \leq \alpha \leq 2.0$ and $\gamma \geq 0$.

Finally, the UV luminosity for each galaxy can be directly related with SFR according to Madau et al. (1998). This model is accurate within the range of $10^8 - 10^9$yr (Kennicutt 1998). The relation between UV luminosity and Star Formation Rate is given by:

$$\mathrm{SFR}\left(M_{\odot}\mathrm{yr}^{-1}\right) = 1.4 \times 10^{-28} L_{\nu}\left(\mathrm{erg\ s^{-1}Hz^{-1}}\right) \tag{7}$$

3.4. *The Luminosity Model*

In this model we have made two assumptions:

1. Each halo in the catalog hosts one galaxy. There are not empty halos, also none of halos has two or more galaxies.
2. The UV luminosity of each galaxy is function of one variable: the mass of the DMH in wich is located.

Our model is a four parameter function. Each galaxy has a luminosity given by:

$$L = L_0 M\left[\left(\frac{M}{M_0}\right)^{-\beta} + \left(\frac{M}{M_0}\right)^{\gamma}\right]^{-1} \tag{8}$$

	Dust Att.		No-Dust Att.	
Parameter	MCMC	C.Var.	MCMC	C.Var.
$\log_{10}(L_0/L_\odot)$	$18.07^{+0.10}_{-0.06}$	0.03	$17.81^{+0.12}_{-0.08}$	0.02
$\log_{10}(M_0/M_\odot)$	$11.19^{+0.67}_{-0.03}$	0.07	$11.12^{+0.58}_{-0.24}$	0.06
β	$1.480^{+0.11}_{-1.28}$	0.18	$1.44^{+0.16}_{-1.35}$	0.18
$\gamma \times 0.1$	$4.028^{+3.01}_{-0.82}$	0.58	$5.18^{+2.36}_{-0.59}$	0.46

TABLE 1
Best fit parameters to the Willott data with and without dust attenuation over 64 small boxes. Mean best value estimated with MCMC, mean 1σ confidence interval and Cosmic Variance (C.Var.)

where M is the hosting DMH mass, L_0 is a normalization constant, M_0 is the critical mass where the luminosity function has a slope change, β and γ are the slopes. This equation has a similar fashion to the mass to light relation (van den Bosch et al. 2003) and the mean relation between stellar mas of a galaxy and the mass of its halo used by Moster et al. (2010).

There exists more sophisticated models as Lee et al. (2009) shown, with scattering in the DM Mass-Stellar Mass, but also including some randomization in star forming histories, starburst episodes (duty cycle); galaxies have not synchronization on the beginning of star forming stage, also this stage may be time limited. It results in the existence of massive galaxies in the studied volume, but with no emmission in the UV continuum due their duty cycle may has not started as well it may ended. Also may be present a normal distribution of the luminosity around the expected values.

4. RESULTS

4.1. *Willott*

We performed MCMC runnings with 100.000 steps over the 64 small cubic boxes (of 250 h^{-1}Mpc side length) fitting the LF to the Willott observational data, comparing the two cases; with and without dust attenuation. (figures 3 and 4). We used the Likelihood Ratio criterion ($\mathcal{LR} = 0.5$) to define the 1σ confidence interval for our parameters.

M_0 is quite similar in booth cases (they are compatible within the error bars), the turnover point corresponds to the same mass. γ and L_0 shown a significative difference in booth cases. β is hard to constraint in booth cases. The parameer was limited to vary in the range form 0.0 to 1.6. 1σ region covers the whole range.

The UV luminosity model (eqn. 3) that we have chosen can be divided in two regimes; high mass regime (with $M > M_0$) and low mass regime (with $M < M_0$).

The observational dataset from Willott are in the high mass regime with one point in the low mass regime. It makes makes hard to impose restrictions over β, but the other three parameters can be well defined.

We also compare the likelihood of the two cases on each individual small box. The Dust Attenuation model is more acurrate than the No-Dust Attenuation model in most of the cases as is shown in the figure 2.

To study cosmic variance effects, we compared the best fit parameters of each box and its likelihood value. We found that cosmic variance effects are less significative in best fit parameters than MCMC parameter estimation itself.

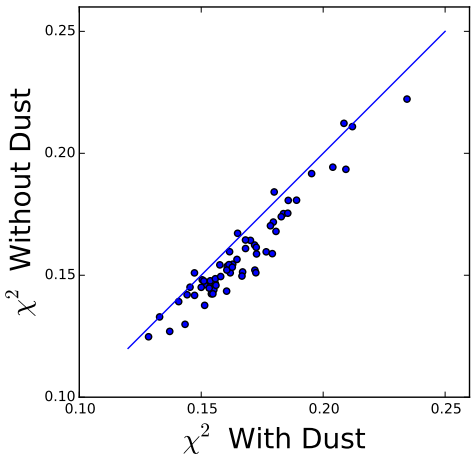

Fig. 2.— Best fit to Willott comparison between the two models. Each point represent χ^2 calculated over each small-box. The solid line represents the ratio 1:1

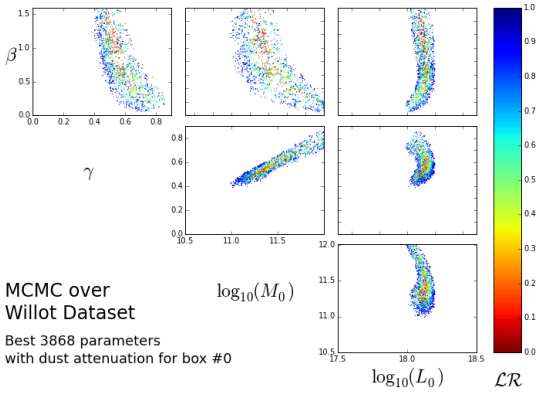

Fig. 3.— Parameter dispersion fitting the Willott with the Dust Attenuation model. 1σ is defined by the likelihood ratio between 0.0 (red) and 0.5 (green)

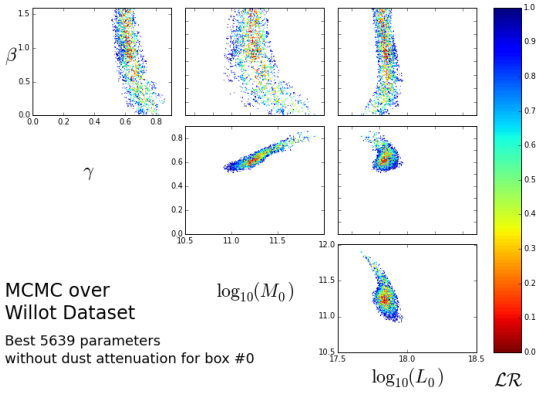

Fig. 4.— Parameter dispersion fitting the Willott with the No-Dust Attenuation model. 1σ is defined by the likelihood ratio between 0.0 (red) and 0.5 (green)

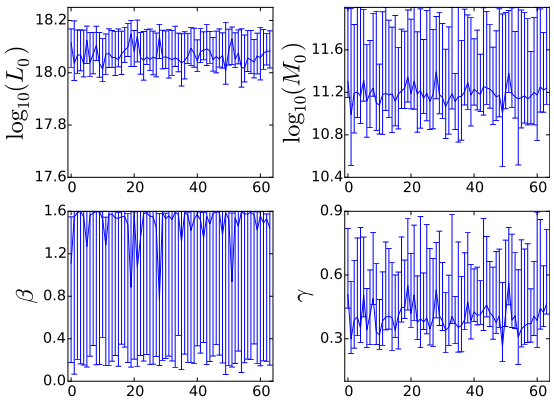

FIG. 5.— Individual small-box parameter estimation with dust attenuation: Best fit values to the Willott data set (solid line) and 1σ confidence interval using likelihood ratio $\mathcal{LR} = 0.5$. The x axis corresponds to the box number.

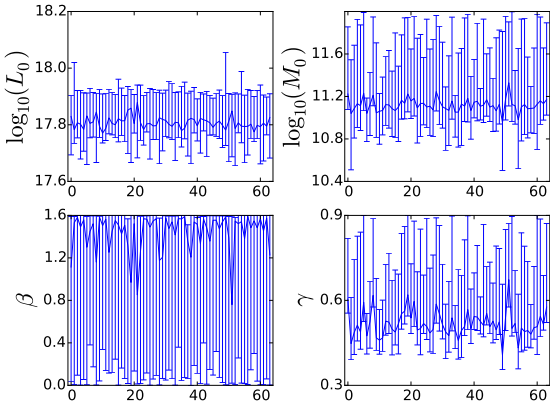

FIG. 6.— Individual small-box parameter estimation with no-dust attenuation: Best fit values to the Willott data set (solid line) and 1σ confidence interval using likelihood ratio $\mathcal{LR} = 0.5$. The x axis corresponds to the box number.

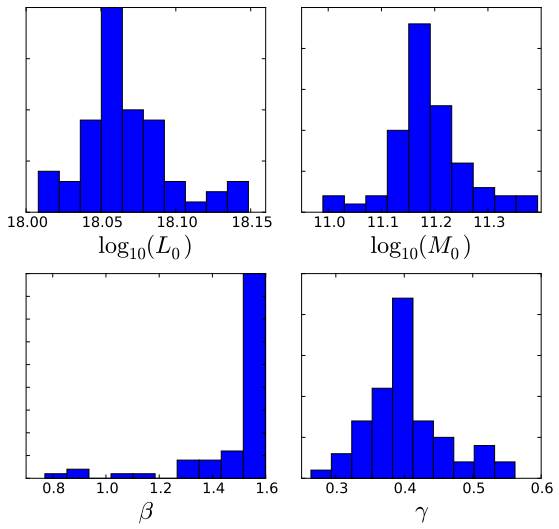

FIG. 7.— Best fit parameter distribution due cosmic variance with Willott data in the dust attenuation model.

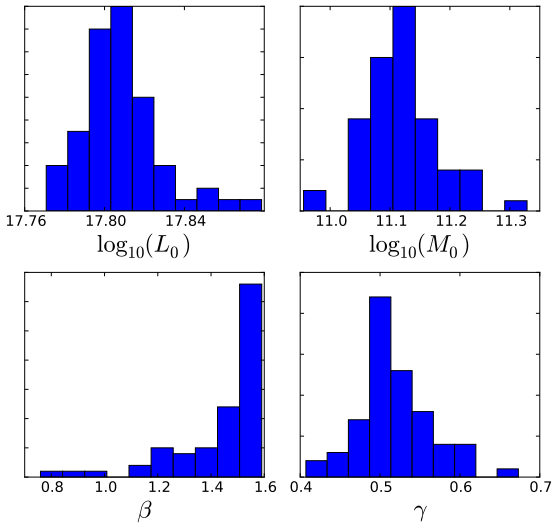

FIG. 8.— Best fit parameter distribution due cosmic variance with Willott data in the no-dust attenuation model.

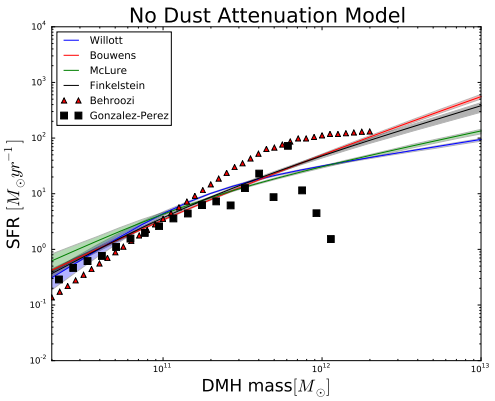

FIG. 9.— Star formation rate as function of the dark matter halo mass without dust attenuation. Solid lines represents the mean SFR value over the small boxes within 50% shaded region. Comparison with the GALFORM semi-analitical model (Gonzalez-Perez et al. 2014) and a implementation of abundance matching model (Behroozi et al. 2013).

5. DISCUSSION

6. CONCLUSIONS

ACKNOWLEDGMENTS

Acknowledgments...

REFERENCES

Behroozi, P. S., Wechsler, R. H., & Conroy, C. 2013, ApJ, 770, 57

Bouwens, R. J., Illingworth, G. D., Oesch, P. A., Franx, M., Labbé, I., Trenti, M., van Dokkum, P., Carollo, C. M., González, V., Smit, R., & Magee, D. 2012, ApJ, 754, 83

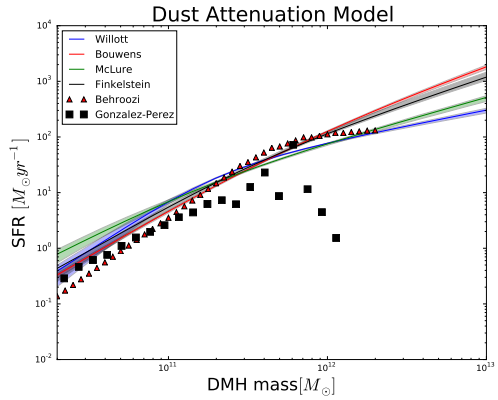

FIG. 10.— Star formation rate as function of the dark matter halo mass with dust attenuation. Solid lines represents the mean SFR value over the small boxes within 50% shaded region. Comparison with the GALFORM semi-analitical model (Gonzalez-Perez et al. 2014) and a implementation of abundance matching model (Behroozi et al. 2013).

Bouwens, R. J., Illingworth, G. D., Oesch, P. A., Trenti, M., Labbé, I., Bradley, L., Carollo, M., van Dokkum, P. G., Gonzalez, V., Holwerda, B., Franx, M., Spitler, L., Smit, R., & Magee, D. 2015, ApJ, 803, 34

Colín, P., Klypin, A. A., Kravtsov, A. V., & Khokhlov, A. M. 1999, ApJ, 523, 32

Conroy, C., Wechsler, R. H., & Kravtsov, A. V. 2006, ApJ, 647, 201

Efstathiou, G., Ellis, R. S., & Peterson, B. A. 1988, MNRAS, 232, 431

Finkelstein, S. L., Ryan, Jr., R. E., Papovich, C., Dickinson, M., Song, M., Somerville, R., Ferguson, H. C., Salmon, B., Giavalisco, M., Koekemoer, A. M., Ashby, M. L. N., Behroozi, P., Castellano, M., Dunlop, J. S., Faber, S. M., Fazio, G. G., Fontana, A., Grogin, N. A., Hathi, N., Jaacks, J., Kocevski, D. D., Livermore, R., McLure, R. J., Merlin, E., Mobasher, B., Newman, J. A., Rafelski, M., Tilvi, V., & Willner, S. P. 2014, ArXiv e-prints

Gonzalez-Perez, V., Lacey, C. G., Baugh, C. M., Lagos, C. D. P., Helly, J., Campbell, D. J. R., & Mitchell, P. D. 2014, MNRAS, 439, 264

Jones, E., Oliphant, T., Peterson, P., et al. 2001–, SciPy: Open source scientific tools for Python

Kennicutt, Jr., R. C. 1998, ARA&A, 36, 189

Klypin, A., Yepes, G., Gottlober, S., Prada, F., & Hess, S. 2014, ArXiv e-prints

Klypin, A. A., Trujillo-Gomez, S., & Primack, J. 2011, ApJ, 740, 102

Kravtsov, A. V., Berlind, A. A., Wechsler, R. H., Klypin, A. A., Gottlöber, S., Allgood, B., & Primack, J. R. 2004, ApJ, 609, 35

Lee, K.-S., Giavalisco, M., Conroy, C., Wechsler, R. H., Ferguson, H. C., Somerville, R. S., Dickinson, M. E., & Urry, C. M. 2009, ApJ, 695, 368

Madau, P., Pozzetti, L., & Dickinson, M. 1998, ApJ, 498, 106

McLure, R. J., Cirasuolo, M., Dunlop, J. S., Foucaud, S., & Almaini, O. 2009, MNRAS, 395, 2196

Meurer, G. R., Heckman, T. M., & Calzetti, D. 1999, ApJ, 521, 64

Moster, B. P., Somerville, R. S., Maulbetsch, C., van den Bosch, F. C., Macciò, A. V., Naab, T., & Oser, L. 2010, ApJ, 710, 903

Pérez, F., & Granger, B. E. 2007, Computing in Science and Engineering, 9, 21

Planck Collaboration, Ade, P. A. R., Aghanim, N., Armitage-Caplan, C., Arnaud, M., Ashdown, M., Atrio-Barandela, F., Aumont, J., Baccigalupi, C., Banday, A. J., & et al. 2014, A&A, 571, A16

Prada, F., Klypin, A. A., Cuesta, A. J., Betancort-Rijo, J. E., & Primack, J. 2012, MNRAS, 423, 3018

Riebe, K., Partl, A. M., Enke, H., Forero-Romero, J., Gottlöber, S., Klypin, A., Lemson, G., Prada, F., Primack, J. R., Steinmetz, M., & Turchaninov, V. 2013, Astronomische Nachrichten, 334, 691

Schmidt, M. 1968, ApJ, 151, 393

Smit, R., Bouwens, R. J., Franx, M., Illingworth, G. D., Labbé, I., Oesch, P. A., & van Dokkum, P. G. 2012, ApJ, 756, 14

Steidel, C. C., Giavalisco, M., Pettini, M., Dickinson, M., & Adelberger, K. L. 1996, ApJ, 462, L17

van den Bosch, F. C., Yang, X., & Mo, H. J. 2003, MNRAS, 340, 771

Willott, C. J., McLure, R. J., Hibon, P., Bielby, R., McCracken, H. J., Kneib, J.-P., Ilbert, O., Bonfield, D. G., Bruce, V. A., & Jarvis, M. J. 2013, AJ, 145, 4